

CALIFORNIA PATH PROGRAM
INSTITUTE OF TRANSPORTATION STUDIES
UNIVERSITY OF CALIFORNIA, BERKELEY

Develop Precision Docking Function for Bus Operation

Han-Shue Tan

**California PATH Research Report
UCB-ITS-PRR-2003-11**

This work was performed as part of the California PATH Program of the University of California, in cooperation with the State of California Business, Transportation, and Housing Agency, Department of Transportation; and the United States Department of Transportation, Federal Highway Administration.

The contents of this report reflect the views of the authors who are responsible for the facts and the accuracy of the data presented herein. The contents do not necessarily reflect the official views or policies of the State of California. This report does not constitute a standard, specification, or regulation.

Final Report for MOU 397

March 2003

ISSN 1055-1425

Develop Precision Docking Function for Bus Operation

Final Report MOU 397

Han-Shue Tan

California PATH

University of California at Berkeley

1357 S. 46th Street, Richmond, CA 94804-4698

hstan@path.berkeley.edu

Abstract

This project is a one-and-half year research and experimental effort to investigate the implementation of the precision docking system on a bus and to demonstrate that the system can provide superior docking accuracy. Since a bus cannot be secured for docking experiments during the period of the project, the Buick LeSabre test vehicle was used to further the docking system development. The work included (1) complete control analysis and integrate docking algorithm with lane-keeping algorithm; (2) software development that integrated the modularized new signal processing algorithm with the docking control algorithm structure; (3) steering actuator performance/component requirements for the automated docking function; (4) feasibility investigation of using driver guidance display for docking maneuver via a driver-in-the-loop display simulator; (5) formulation of the automated-manual transitioning problem and the design of a transition controller; (6) demonstration of precision docking.

The research completed under this project contributed to three sets of deliverables: (1) a final report which presents the analysis and experimental results of the development of the integrated lateral control system based on the magnetic marker for both precision docking and lane-assist functions, (2) requirements for steering actuator design, and (3) demonstrations of precision docking and lane-assist control using Buick LeSabre test vehicle.

1 Executive Summary

This project is a one-and-half year research and experimental effort, which investigates the implementation of the bus precision docking system and to demonstrate the superior docking accuracy. This report focuses on the analysis and experimental results of the development of an integrated lateral control system using magnetic marker for both precision docking and lane-assist functions.

Bus Rapid Transit (BRT) is an effective alternative for providing rail-like corridor transit service. An advanced BRT concept involves the use of automated buses to provide functions of a rail transit system. A vehicle under automatic steering control following a prescribed trajectory is operated like a train on a rail. A lateral position sensing that uses roadway markers, such as magnetic markers embedded under the roadway, as lateral reference is a one of the promising approaches for a reliable sensing system. The BRT concept requires the steering control system to consistently perform all necessary steering functions from high speed driving to low speed precision docking. This report describes the design of a single steering controller that achieves all performance objectives. Data collected during public demonstrations are presented in this report to illustrate the effectiveness of the results.

Transit services will expand from the traditional grid operations to provide more transportation options. Notably, Bus Rapid Transit (BRT) will offer commuters more convenient and reliable service. BRT will be operated on dedicated rights-of-ways along congested corridors to connect employment, business and residential concentrations. BRT has the advantages of rail transit for reliable and high frequency service. It also has the flexibility to operate outside the corridors and in various express patterns potentially for 'door-to-door' service. The capital, operation and maintenance costs for BRT using vehicle-highway automation technologies will be significantly lower than for rail transit systems. BRT features can help attract significant commuters from single occupancy vehicles, which will ultimately contribute to the reduction of traffic congestion on the

corridor. The BRT capabilities can be extended from full-size buses to smaller buses and other high-occupancy vehicles (HOVs), including carpools and vanpools.

The convenience and reliability of BRT operation will be enhanced by the application of automated steering technologies. BRT vehicles can be automatically guided within the corridor and operated on much narrower lanes on an electronic 'guideway'. Automated precision docking together with alternative bus designs (e.g. low floor and large doors) will offer fast and convenient passenger loading/unloading at the platforms; therefore stop times will be reduced. When operated outside of the corridor, buses can be either manually controlled or operated using electronic guidance.

The targeted automated steering control systems for BRT have the following strong requirements: high reliability, high precision, high speed operation, high adaptability to various operating conditions, as well as high passenger comfort. To facilitate the above goals, a complete automatic lateral control system needs to reliably perform all of the following basic functions: reference path definition, sensing and signal processing, control, and actuation.

The roadway is either defined by markers on the roadway or stored in memory devices such as maps or tables. Different markers have been proposed: magnet nails or strips, electric wires, resonance coils, guard rails, different radar reflectors (strip, paint, mesh), optical or electro-optical reflectors, acoustic or ultrasonic reflectors, or ordinary lane markers. Differential GPS (DGPS) and map, possible aided by Inertial Navigation System (INS), can also be used as the lane reference system. Each lateral reference system is based on specific detection devices, media, and technologies. In this project, a lateral referencing system based on magnetic roadway markers is chosen as the default sensing system because of its simplicity and reliability for both bus docking and lane assist functions.

PATH has developed a precision docking function. The system consists of roadway markings and on-vehicle control system. The roadway markings use a sequence of magnetic markers (permanent magnets) to define the vehicle trajectory. The on-vehicle

control system includes magnetic sensors, a steering actuator, and a control computer. Although the project proposal proposes to implement this precision docking system on a bus, a test bus was not able to be secured for such implementation and testing during the period of the project. LeSabre test vehicle was then proposed to be the platform for continuing the development and understanding of the precision docking functions and performances.

The original project incorporates four tasks:

- Task 1 comprised the development of hardware for the bus for the precision docking functions.
- Task 2 comprised the development of software for the lateral sensing system and control for precision docking.
- Task 3 comprised development of Human Machine Interface for driver to engage and disengage docking functions.
- Task 4 comprised demonstration and experimental evaluation of the precision docking systems.

Task 1 studied the hardware development for the precision docking system. Since a bus could not be obtained from a transit agency during the project period, this task was focused on the following sub-tasks that were crucial for the precision docking hardware development: developing a preliminary steering actuator requirements; designing a smart steering actuator servo; increasing the magnetometer sensor range; and creating temporary surface-mount magnets for docking testing.

A clear understanding of the steering actuator bandwidth requirement is an important piece of information before installation of a new steering actuator on a bus when no such commercial actuator is available. The Buick LeSabre test vehicle became a useful tool for such evaluation during especially when bus was not available. A steering actuator with bandwidth better than 5 Hz was installed in the LeSabre. A low-pass filter was added to the steering command to imitate a slower actuator with lower bandwidth. The observation

from the test results suggested that a 2-3 Hz actuator could perform the docking function quite well based on the initial results from the LeSabre docking experiments. Section 2 reports the preliminary requirements for the precision docking bus steering actuator.

The specification of the functional requirements for the actuator was based on the assumption that the steering actuator is mechanically attached to the steering column located in between the original hydraulic power steering assist output and the torsion bar. In such configuration, the steering actuator can be treated as an add-on device with lower power and torque capabilities. Although the final selection about the steering actuator configuration as well as hardware has not been determined, a new software driver has been designed. Effort has been made to keep the software structure and driver as generic as possible to improve their portability should a different steering actuator hardware be chosen in the future. The ideal functional requirements for the bus docking actuator include the following functional blocks:

- Initialization subroutine.
- Calibration subroutine.
- Transition subroutine.
- Servo subroutine.
- Fault detection/management subroutine.

Although LeSabre can perform the basic docking function with the current 3-magnetometer lateral sensor configuration, bus docking, especially under the S-type curve maneuver, requires much larger sensor range since the wheel base is significantly larger than that of a passenger vehicle. A new 5 to 7-magnetometer lateral sensor configuration was developed to anticipate the future implementation of sensors for bus docking. Two-to-four additional magnetometers were incorporated to extend the sensor range to 150-to-210 centimeters, which is necessary for performing a sharp S-curve docking. The increased sensor range is designed to cover the large offset-tracking difference between the front and rear wheel when a bus is negotiating a sharp curve. PATH has also investigated the associated wiring as well as the appropriate A/D board connection for such installation.

A temporary magnetic marker trail is very useful to evaluate different target trajectories for bus docking. A method that facilitates temporary installation of surface-magnets for docking demonstration and testing was therefore developed. One-inch diameter rare-earth magnets were encased in plastic resin to provide more road surface contact area and a “softer” profile in the event a car rolled over a marker. Contact adhesive can be used to fix the markers in place during the testing or demonstration period. A “smoothing computation” is developed in the signal-processing algorithm to allow the use of a single magnetic table for both one rare-earth or four ceramic magnetic markers. Such temporary marker system has demonstrated docking accuracy of better than 1 centimeter with a Buick LeSabre simulating a bus.

Task 2 focused on the development of data processing and control software for precision docking. It includes the design of a unified software structure for bus docking as well as for general lane-assist functions. The real-time software for vehicle lateral control is developed using C programming language under the QNX operating system environment. The functions of the real-time software are to process the signals obtained from the sensors; give the steering control command as well as the display and warning signals based on those signals; send either the steering control command to the steering actuator, or the display and warning signals to the human machine interface. Refer to Fig. 1.1 for the basic software structure.

To achieve those functions, the real-time software was structured in the following five basic component groups: lateral control module, guidance and warning module, human machine interface, device driver and database manager. Fig. 1.2 shows the function of and interaction between those software components.

- Lateral Control Module: The steering control module retrieves sensor signals from the database, processes sensor signals, calculates the steering command, and writes the steering command to the database.

- Guidance and Warning Module: The guidance and warning module retrieves sensor signals from the database, calculates the guidance parameters and the warning signal, and writes them to the database.
- Human Machine Interface: The human machine interface displays the parameters used for guidance and warning.
- Device Driver: The device drivers, which are running in background when the control program is invoked, handle all the communication with the data acquisition boards and the RS232 board. The device drivers gather sensor signals from the magnetometers every 2 msec and write them to the database.
- Database Manager: The database manager maintains a set of variables, which are updated or retrieved by the device drivers, the lateral control module, the guidance and warning module, and the human machine interface.

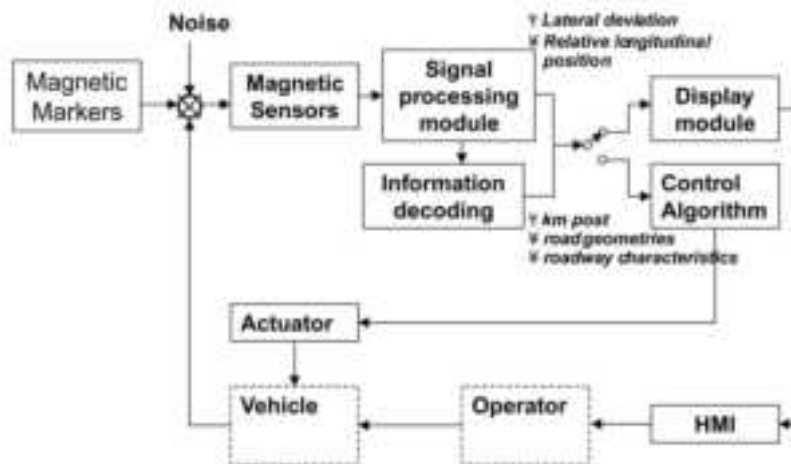


Fig. 1.1 Docking Steering Control Functionality

The development of a modularized magnetic signal-processing algorithm (see Section 3 for detailed description of the algorithm) is also an important issue of Task 2. A new modularized magnetic signal-processing algorithm that includes the use of the longitudinal field strength for peak detection is also investigated in this project.

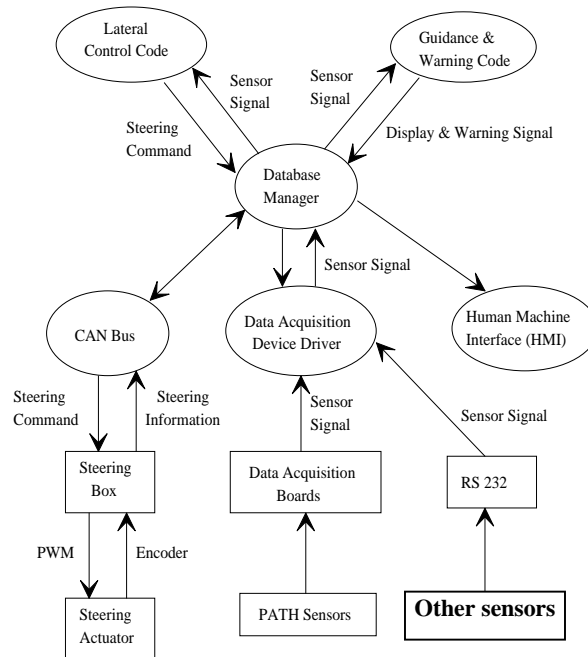


Fig. 1.2 Software Components Interaction

Reliable and modularized lateral software is crucial for long-term lateral control system development and sensor integration. PATH has determined to use a three-magnetometer sensor combination for the LeSabre docking demonstration. In order to provide smooth transition among three magnetometers that is essential for the low-speed docking maneuver, PATH has also developed necessary software for switching among these sensors. The reconstructive software development tool that was developed through MOU 250 has been extended for the docking sensor calibration. An automated process for magnetometer table calibration was developed to speed up the calibration process. The “reconstructive” software system was developed to improve the reliability and reduce the development time of the lateral sensing system with the magnetic road markers. The reconstructive development tool generated the identical signal processing software in a laptop computer as the one ran in the real-time vehicle environment in the same QNX operating system. The inputs to this software were all the sensor data that stored during real vehicle testing. In such setup, any erroneous situation can be recreated in a lab environment and debug with ease. PATH has also linked the extensive Matlab data processing ability to this tool in a laptop computer so that the debugging process could be automated. With this development environment, PATH staff could (1) capture the

problematic performance as soon as it happens, (2) recreate the situation step by step in the lab environment, and (3) modify the software as well as validate the changes before upgrading the new version of software in the test vehicle. This tool will significantly shorten the development time for the integrating the new magnetometer configuration to the bus precision docking once the bus is obtained.

Task 3 studied the Human Machine Interface that assists driver to engage/disengage the docking operations. The work consists of (1) designing a simple guidance display that assists the operator for automated/manual transition; (2) utilizing a driver-in-the-loop simulation to assess the performance difference between driver assistance and automated precision docking.

The likely automated bus docking application during the initial phase involves manual to automated transitioning. Bus driver would operate the vehicle manually until he approaches the final docking station. He/she will then activate the automated docking function and transition the bus into the automated steering mode to bring it parallel to the docking station with high accuracy. The key to a successful transition depends on both the smoothness and the robustness of such transition. PATH has formulated the transitioning problem and designed a transitioning controller for such maneuver.

To evaluate the effective of the precision docking performance, a guidance display screen design has been adopted for such study. In the center of the display are two white lines simulating the lane width on the road. At the top is a small blue square, showing where the vehicle will be in 20 meters. At the bottom is a blue rectangle showing the current location of the vehicle in the lane. A message can be displayed below this rectangle. It shows information such as the docking begin, docking end; and the distance left before a right or left turn or docking station.

On the top left corner of the screen is a single letter, showing the current status of the steering system: M for manual driving, G for guidance, A for automated. On the top right corner of the screen is the vehicle speed (in km/h), and on the bottom right corner the distance traveled (in m) since the beginning.

The color of the white lines and red squares change according to the system status. When the system starts, the screen is blank. Once some magnets are read, the road lines and the vehicle positions become yellow. Once a “docking-begin” marker is passed, the road lines become white and the vehicle positions red. If too many magnets are missed, the road lines and the vehicle positions turn gray. Finally, if the system is in automated steering, the road lines are always white and the vehicle positions always blue.

Based on the above guidance display, a driver-in-the-loop display simulator has been developed. A commercial steering wheel for video game is used to imitate a real steering wheel. It sends the operator’s steering angle signal to a desktop computer. A vehicle model in the computer takes this angle information and computes the relative vehicle displacement with respect to the docking trajectory stored in the computer. An algorithm that calculates the appropriate predictive information for bus docking was also developed. A monitor displays both the current vehicle location as well as predictive information to help the operator steer. The operator uses this information to stably perform the docking function. The initial driver-in-the-loop simulation shows that (1) such display can support docking to better than decimeter accuracy; however, (2) driver requires significant attention at the display to perform such function. Such attention may not be acceptable in practice because bus driver needs to address many operational details during docking. Additional human factor evaluation using test vehicle is necessary to further evaluate this finding.

Task 4 consists of design, implementation, demonstration and evaluation of the performance of the automated precision docking system. Without an instrumented bus, LeSabre test vehicle was used for this purpose. The tasks included installation/design of roadway markings at the demonstration sites (first at RFS as well as at other demonstration sites); design and implementation of an integrated docking control algorithm (see Section 4 for the detailed design); and demonstrations (many demonstrations had been performed at RFS during and after the project).

Various control synthesis have been applied to automatic steering control in the past: LQ [1, 2], H_∞ and μ -synthesis [3], linear parameter varying (LPV) [4], classical [5, 6], linear robust control [7], nonlinear optimization [8], backstepping control [9], sliding mode control [10], feed-forward preview control [1, 2], road estimation [11], and adaptive control [12, 13]. Many simulation results show tracking accuracy to sub-centimeters range. However, most papers do not aim at designing a comprehensive controller that can be applied to real scenarios with realistic measurement information. The real-world considerations include vast amount of possible uncertainties as well as the sensitive nature of human perceptions. The good performance presented by many papers often requires either good system models, or specific unmodelled dynamics structure, or accurate measurements, or known vehicle parameters, or ideal steering actuator and mechanism. Some of the controllers perform perfectly under specific design scenarios but with noticeable degradation otherwise.

One of the goals of this report is to present a practical controller design that addresses the real-world vehicle steering control issues that link both precision docking and lane-assist functions. An automated steering control system targeted toward a real-world application, such as in a BRT system, is required to perform all normal steering functions from start to stop with extreme reliability and high performance. The control system should be robust against different roadway geometries, unknown vehicle loading, various speeds, and changing roadway surface conditions. The targeted controller should have a simple control structure and be easy to design, tune and implement. The design presented in the section of this report is based on a classical control approach that focuses on pushing the performance limits without precise model information. The approach aims at achieving high gain with high stability margins, and at handling many operational conditions with limited controller transitions. The unified controller design potentially simplifies the procedure of lateral sensor fusion, another advantage for real-world applications.

Figure 1.3 shows the desired docking trajectory as well as the front and rear sensor measurements during 10 consecutive fully automated docking demonstration runs. These runs were conducted with 0 to 4 passengers. Figure 1.3 clearly shows that once the

docking curve starts at marker number 25, the tracking performance was so consistent that only two trajectory lines (one for front and one for rear) are distinguishable. By blowing up the top plot of Figure 1.3 from marker number 52 to 62 as shown in the bottom plot of Figure 1.3, one can see that the variation at every marker point is within 5 millimeters peak to peak. Moreover, the vehicle stops by the curb within 2-car length with an accuracy of 5 millimeters. The precision docking demonstration shows that the automated docking performance exceeds that from human in precision and consistency either under fully automation where throttle and brake are controlled by computer, or under semi-automation where the driver controls the speed.

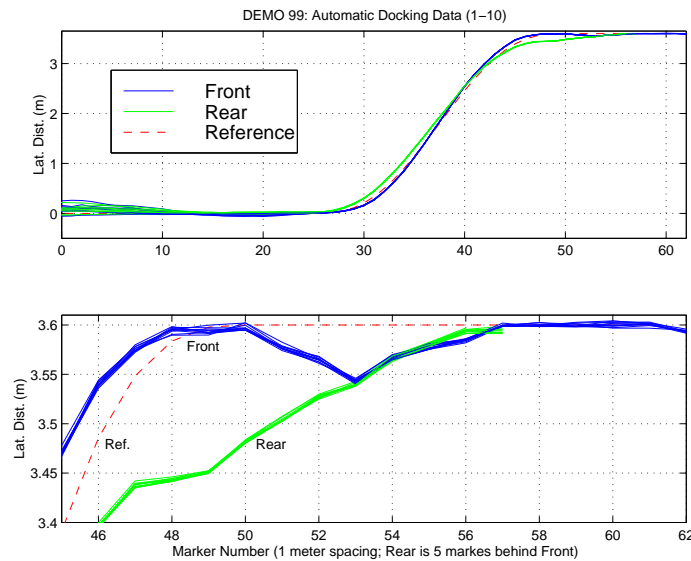


Fig. 1.3 Automatic precision docking demonstration data.

Since the design methodology employed in this report emphasizes on high gain feedback and high stability margins, the commonly used “road preview controller” that feeds forward the road curvature information to steering command does not play a significant role in the design. The experiments repeatedly show that the only noticeable difference between using and not using the road curvature information is during the curve transitions. The maximum transition error without road preview is generally about twice as big as the one using feed-forward control based on road curvature. The analysis results provide good estimates with respect to real-world results.

The following sections detailed the analysis results that support the development of an integrated lateral control system using magnetic marker that perform both precision docking and lane-assist functions.

2 Preliminary Steering Actuator Requirements

2.1 Top level (closed-loop) steering actuator system requirements:

- **Functionality:**

Turn on/off by software

Variable driver resistance capability

High performance steer position servo

Emergency shut-off

Ability to impose small force oscillation on hand wheel

- **Performance:**

Closed loop servo bandwidth: at least 4 Hz for small amplitude

Maximum slew rate: at least 30 degree/sec at the tire (500-600 degree/sec at hand wheel)

No oscillation/vibration on hand wheel

Position servo accuracy: better than 1 degree at hand wheel

Zero position accuracy: better than 1 degree at hand wheel

Control Resolution: better than 0.2 degree at hand wheel

- **Safety**

Fail to no torque

Self diagnosis ability

Max torque/rate/power protection

Kill switch

- **Installation**

Column installation above assist components

Low noise level

- **Input/output**

Input: steering commands (position or torque), on/off command

Outputs: steering position(s), actuator status and/or fault flags

2.2 Component level steering actuator (open loop) specifications:

- Maximum torque: 8-10 N-m
- Maximum slew rate: faster than 25-30 degree/sec at tire (500-600 degree/sec at hand wheel)
- Range: full range of the steering angle
- Position sensor resolution: better than 0.1 degree at hand wheel
- Zero position accuracy: better than 1-2 degree at hand wheel
- Command rate: faster than 100 Hz (if digital), or analog connection between motor circuit and Host computer.
- Time constant for the current/torque command response: faster than 5 ms.
- Fault flag for the open-loop system.
- The motor should be able to be “Back driven” by the driver.

3 Magnetic Sensing Algorithm

There are several algorithms designed to detect the relative position between the marker and sensor (magnetometer), as well as to read the code embedded within a sequence of these markers. Three magnet-marker-detection and mapping algorithms have been experimented by PATH:

- The “peak-mapping” method. It utilizes a single magnetometer to estimate the marker’s relative lateral position when the sensor is passing over the magnet.
- The “vector ratio” method. It requires a pair of magnetometers to sample the field at two locations and returns a sequence of lateral estimates in a neighborhood surrounding, but not including the peak.
- The “differential peak-mapping” algorithm. It compares the magnetic field measurements at two observation points to eliminate the common-mode contributions

and reconstructs a functional relationship between the differential sensor readings and the lateral position using the knowledge of the sensor geometry.

The “peak-mapping” algorithm is chosen for the precision docking project because it has been proven effective over a wide range of speeds and it is less sensitive to the possible local magnetic field variations from the bus platform.

Under the assumption that the vehicle lateral speed is significantly smaller than that of the vehicle longitudinal velocity, it is obvious that the largest vertical field B_z occurs at the point when the sensor is just passing over the magnetic marker, i.e. as $x=0$. This point is called “peak” because it corresponding to the point where the magnetic field achieves its maximum during its trajectory around the magnetic marker in question. The most important fact is that the three dimensional mapping can be reduced to a two-dimensional mapping using the constraint relationship under the magnet at $x=0$.

Two basic methods can be used to detect the peaks: the variance method (using B_z) and the switching (using B_x) method. The variance method computes the instantaneous variance of the vertical field $\sigma_z(t_k)$ as

$$\sigma_z(t_k) = \sum_{i=k-N}^k (B_z(t_i) - \bar{B}_z(t_k))^2 \quad (3.1)$$

where $\bar{B}_z(t_k)$ is the running average of the last N samples, i.e.,

$$\bar{B}_z(t_k) = \frac{1}{N} \sum_{i=k-N}^k B_z(t_i). \quad (3.2)$$

Using this variance, the peak and the valley of the vertical field can be identified using the following relationship

$$\text{if } |B_z(t_k) - \hat{B}_{zEarth}| > HIGH_threshold \ \& \ \sigma_z(t_k) < \varepsilon \Rightarrow \text{Peak detected}, \quad (3.3)$$

$$\text{if } |B_z(t_k) - \hat{B}_{zEarth}| < LOW_threshold \ \& \ \sigma_z(t_k) < \varepsilon \Rightarrow \text{Valley detected}. \quad (3.4)$$

Equation (3.4) suggests that the marker is far away enough to the sensor that the field from the magnetic marker is negligible. Thus the earth field estimates (B_{zEarth}, B_{yEarth}): vertical and horizontal earth field, can be updated based on the sensor measurements at

the valley. It should be noted that the earth estimates play a very important role in the accurate computation of the lateral deviation.

To improve the reliability of the peak detection process, the switching method utilizes the sign-change property of the longitudinal field (B_x) at peak both to provide candidates for peaks and to double-check any detected peak.

Once the peak is detected and the marker's magnetic field is computed as

$$B_{zMar\ ker} = B_z(t_m) - \hat{B}_{zEarth}, \text{ and } B_{yMar\ ker} = B_y(t_m) - \hat{B}_{yEarth}. \quad (3.5)$$

By setting $x=0$ on Equation (3.2), the slope function between the vertical and horizontal field of $\vec{B}_{Mar\ ker}$ can be expressed as

$$\frac{B_{zMar\ ker}}{B_{yMar\ ker}} = \frac{2z^2 - y^2}{3yz} \equiv \varphi(y, z). \quad (3.6)$$

It is known from calculus that the curve (B_z, B_y) form a field if $\varphi(y, z)$ is single-valued, or that partial derivatives of $\varphi(y, z)$ do not vanish. Since

$$\frac{\partial^2 \varphi(y, z)}{\partial y \partial z} = \frac{y^2 - 2z^2}{3y^2 z^2} \neq 0, \text{ as long as } y \neq \sqrt{2}z, \quad (3.7)$$

under the restriction that $y \in \{y_{\min}, y_{\max}\}$ and $z \in \{z_{\min}, z_{\max}\}$, with $z_{\min} > 0$ and $y_{\max} < \sqrt{2}z_{\min}$, the curve $\{B_{yMar\ ker}, B_{zMar\ ker}\}$ does form a field. Therefore, the inverse mapping from $\{B_{yMar\ ker}, B_{zMar\ ker}\}$ to $\{y, z\}$ does exist for most of our application where z_{\min} is usually greater than 15 cm and y_{\max} is less than 20 cm.

A typical inverse map is shown in Fig. 3.1 where two sets of calibration data, one at 9 centimeter height and the other at 11 centimeter, for the vertical and horizontal field of the marker are collected at the interval of every 2 centimeter lateral displacement. One advantage of this method is its robustness against height variations. Observe from Fig. 3.1 that changes in z only serves to move the coordinates along the radial lines that denote constant y .

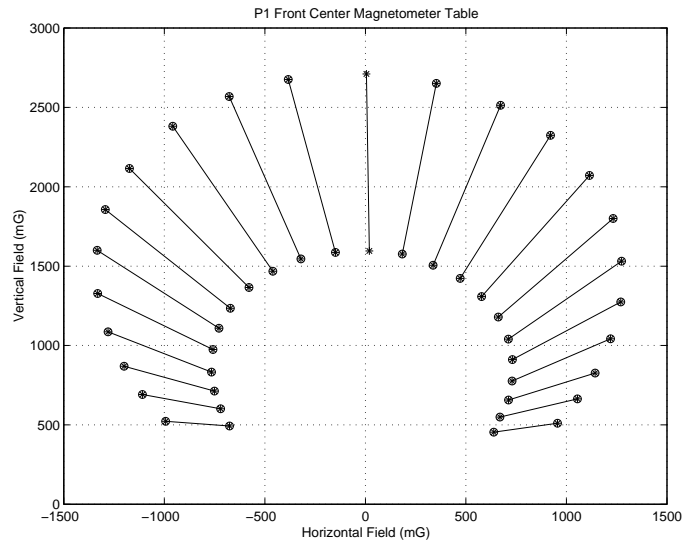


Fig. 3.1 LeSabre Front Center Magnetic Table

Finally, the signal processing for the “peak-mapping” method combine the following three procedures: peak detection, earth field removal and lateral displacement table look-up as shown in the block diagram in Figure 3.2.

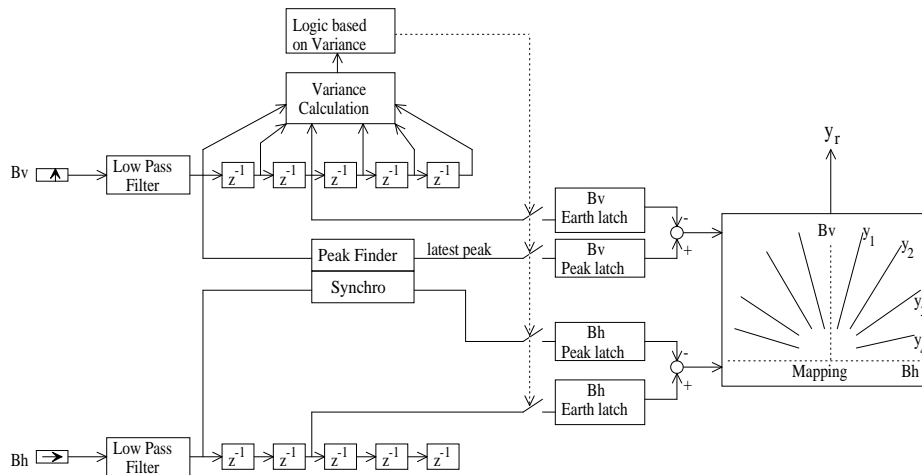


Figure 3.2 “Peak-Mapping” Magnetometer Signal Processing Block Diagram

4. A Uniform Automatic Steering Design for Precision Docking & Lane Assist Functions

4.1 Problem Formulation and Vehicle Model

4.1.1 Performance Requirements

An automated steering control system targeted toward a BRT application is required to perform all normal steering functions from leaving a bus station to arriving at a bus station with extremely high reliability. It should be robust against different roadway geometries, unknown vehicle loading, various speeds, and changing roadway surface conditions. An ideal element of such automated steering control system is a high-gain robust “vehicle lateral servo” that “steers” the vehicle to follow any desired trajectory as long as such trajectory is defined within the limitations of the vehicle capabilities. The closed-loop performance requirements for all possible scenarios are defined as follows:

- 0.2 meter maximum tracking error for highway driving without any prior knowledge of the roadway;
- 0.5 meter maximum tracking error for 0.3-g automated steering maneuver without any prior knowledge of the roadway;
- 0.02 meter maximum tracking error for speeds less than 5 m/s on straight sections of the roadway for docking accuracy;
- no noticeable oscillations at frequencies above 0.3 Hz for passenger comfort, and 0.4 minimum damping coefficient for any mode at lower frequencies;
- 1 m/s² maximum lateral acceleration deviation between the lateral acceleration created by the vehicle and that from the road;
- consistent performance under various vehicle-operating conditions.

In addition to the above performance requirements, a uniform control structure is preferable since it will not require transition between different controllers. The transitions between different controllers usually increase the complexity of the controller design, and often reduce the robustness of the overall system. This design preference pushes for a

single controller that works for all four scenarios without any transitioning between different control configurations.

4.1.2 Vehicle Steering Model including Suspension Mode

Many researchers have used the bicycle model [1] to design steering controllers with various successes. Experimental data for vehicles with soft suspensions, however, suggest that suspension dynamics does contribute to a significant deviation in the frequency response from steering input to lateral acceleration to that from the prediction of the bicycle model [14]. The frequency usually exhibits lower gain characteristics and larger phase lag over the suspension frequency range. The experiments presented in this report were conducted using a Buick LeSabre, a full-size sedan with relatively soft suspensions. This vehicle is equipped with a lateral accelerometer and a yaw rate sensor that are both installed around the vehicle's CG. By using the frequency sweep technique, the experimental open-loop frequency responses from steering angle to lateral acceleration and yaw rate can be obtained. They are shown in Figure 4.1(a) at three different velocities: 10, 20, and 30 m/s. As seen in the figure, the gain of the frequency response for lateral acceleration drops over the frequency range around 2Hz. This is a phenomenon that cannot be predicted by the bicycle model.

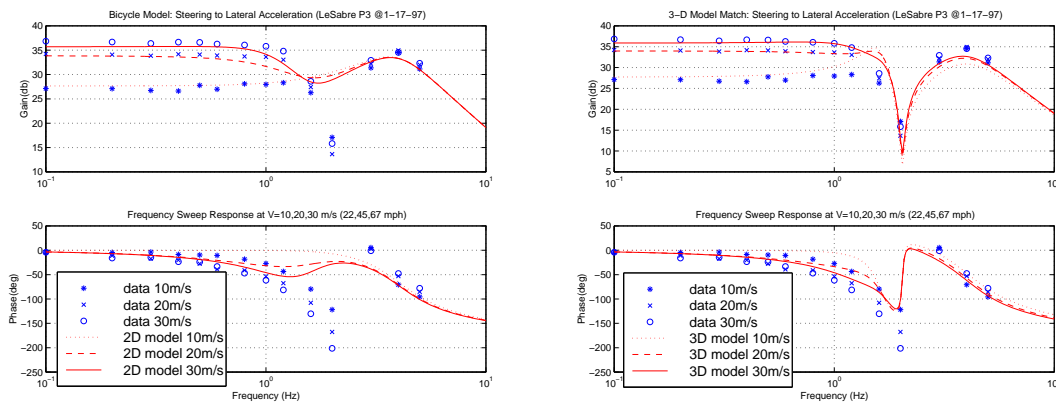


Fig. 4.1. Test vehicle (LeSabre) open-loop transfer function from steering to lateral acceleration. (a) Left: bicycle model; (b) Right: 3 DOF model.

In order to study the influence of the suspension roll dynamics on the steering control design, a 3 DOF vehicle model that includes lateral, yaw and roll dynamics is developed.

Under constant speed condition, the dynamic equations of motion are derived using the Newtonian method as in [14]. The schematic diagram of the 3 DOF vehicle model is shown in Figure 4.2. The sprung mass (m_s) interacts with the front and rear unsprung masses via the front and the rear suspensions, where K_f, D_f and K_r, D_r are the rotational spring and damper coefficients for front and rear suspension, respectively. The roll axis is defined as the line connecting the roll centers of the front and rear suspension. One can find that the vehicle geometric parameter that affects the coupling between lateral and roll dynamics the most is h_{m_s} , the distance between the sprung mass CG and the roll axis.

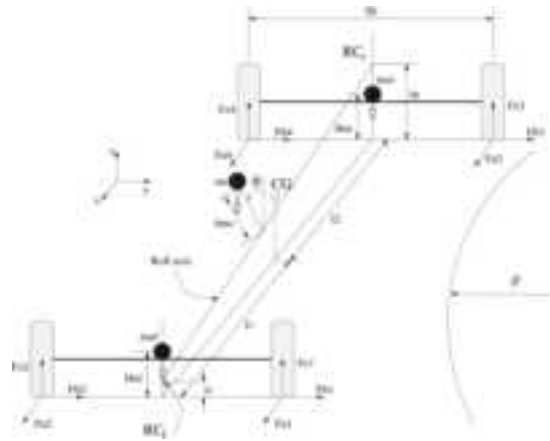


Fig. 4.2. Schematic diagram of 3 DOF vehicle model.

Assuming small angles and using the linear tire model, Eq. (4.1) is the linear vehicle equations with respect to the road reference frame as derived in [14]. The state-space representation takes the form of $\dot{\bar{x}} = A\bar{x} + B\delta + \bar{d}$. The state variables are: y_r, \dot{y}_r , the lateral displacement at CG w.r.t. road reference frame and its derivative; $\psi_r, \dot{\psi}_r$, the yaw angle w.r.t. the road reference frame and its derivative; as well as $\phi_r, \dot{\phi}_r$, the roll angle and its derivative. The road reference frame is attached to the road center at a point adjacent to the vehicle CG with X axis tangent to the road trajectory and moves along the road with the same speed as the vehicle. The input is the front steering angle (δ). The disturbances are: ρ , the road curvature; $\dot{\psi}_d$, the desired yaw rate from the road; F_{wy} , the disturbance force at CG along the y direction; and F_x , the front tire force along the tire orientation. Table 4.1 lists the variables and parameters (including the steering actuator) that were identified by the test data. Figure 4.1(b) shows a significant better match with

the test data at the suspension frequency from the 3 DOF model than that from the bicycle model.

$$\frac{d}{dt} \begin{bmatrix} y_r \\ \dot{y}_r \\ \psi_r \\ \dot{\psi}_r \\ \phi_r \\ \dot{\phi}_r \end{bmatrix} = \begin{bmatrix} 0 & 1 & 0 & 0 & 0 & 0 \\ 0 & \frac{A_1\Lambda_1}{v} & -A_1\Lambda_1 & \frac{A_2\Lambda_1}{v} & R_1 & R_2 \\ 0 & 0 & 0 & 1 & 0 & 0 \\ 0 & \frac{A_3}{v} & -A_3 & \frac{A_4}{v} & R_3 & 0 \\ 0 & 0 & 0 & 0 & 0 & 1 \\ 0 & \frac{A_1\Lambda_2}{v} & -A_1\Lambda_2 & \frac{A_2\Lambda_2}{v} & R_4 & R_5 \end{bmatrix} \begin{bmatrix} y_r \\ \dot{y}_r \\ \psi_r \\ \dot{\psi}_r \\ \phi_r \\ \dot{\phi}_r \end{bmatrix} + \begin{bmatrix} 0 \\ B_1\Lambda_1 \\ 0 \\ B_2 \\ 0 \\ B_1\Lambda_2 \end{bmatrix} \delta + \begin{bmatrix} 0 \\ d_1 \\ 0 \\ d_2 \\ 0 \\ d_3 \end{bmatrix} \quad (4.1)$$

Table 4.1. The 3 DOF vehicle parameters.

Vehicle mass (M)	1740 kg
Sprung mass (m_s)	1600 kg
Front unsprung mass (m_{uf})	80 kg
Rear unsprung mass (m_{ur})	60 kg
Roll inertia (I_{x_s})	420 kg m ²
Yaw inertia (I_{ψ})	3214 kg m ²
Front tire cornering stiffness (c_f)	29000 N/rad
Rear tire cornering stiffness (c_r)	60000 N/rad
Front axle to CG (l_f)	1.058 m
Rear axle to CG (l_r)	1.756 m
Wheel base (S_b)	1.5 m
Roll damping (D_f, D_r)	50 N m sec
Roll stiffness (K_f, K_r)	20000 N m
Sprung mass CG to roll axis (h_{m_s})	0.38 m
Roll steering coefficient (γ)	50
Actuator damping ratio (ξ)	0.4
Actuator natural frequency (ω_n)	5 Hz

4.1.3 Control Problem Formulation

Since most vehicle lateral sensing systems provide lateral measurement at a certain sensor location, the control formulation starts with using such lateral measurement for steering control. Assuming this measurement is taken at a location d_s meters in front of CG, the lateral displacement at the sensor location can be written as

$$y_s = y_r + d_s \psi + h_s \phi, \quad (4.2)$$

where h_s is the distance from the sensor to the roll axis. Differentiating Eq. (4.2) twice and assuming v is constant, the vehicle lateral acceleration transfer function at the sensor location S , $V_s(s)$, is derived by using Eq. (4.2) as

$$y_s(s) = \frac{V_s(s)}{s^2} \delta(s) = \frac{1}{s^2} (s[0 \quad 1 \quad 0 \quad d_s \quad 0 \quad h_s](sI - A)^{-1} B) \delta(s). \quad (4.3)$$

Alternatively, $V_s(s)$ can be defined as

$$V_s(s) = sG_{\dot{y}_r, \delta}(s) + d_s sG_{\dot{\psi}, \delta}(s) + h_s sG_{\dot{\phi}, \delta}(s) \quad (4.4)$$

where $G_{\dot{y}_r, \delta}(s)$, $G_{\dot{\psi}, \delta}(s)$ and $G_{\dot{\phi}, \delta}(s)$ are transfer functions from steering angle to \dot{y}_r , $\dot{\psi}$ and $\dot{\phi}$, respectively.

Figure 4.3 depicts a generic block diagram of a steering feedback system based on lateral displacement measurement. The vehicle lateral model consists of five subsystems: actuator dynamics ($A(s)$), road reference (desired lateral acceleration at the sensor location: $\ddot{y}_{ref} = v^2 \rho$), vehicle dynamics at sensor ($V_s(s)$), vehicle kinematics ($1/s^2$) and control law ($C(s)$). The goal of steering control synthesis is to determine a control law $C(s)$ that is capable of stabilizing the vehicle lateral dynamics with sufficiently high gains to satisfy the performance requirements. One major challenge in choosing the controller $C(s)$ is to maintain enough stability margins under the delays and uncertainties from $V_s(s)$ and $A(s)$.

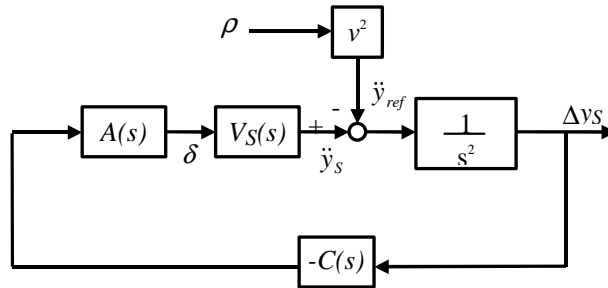


Fig. 4.3. Vehicle steering control block diagram.

4.2 Steering Controller Design

4.2.1 Controller Requirements

The stability and performance requirements are examined for the simplified steering closed-loop system described in Figure 4.3 as

$$\Delta y_s(s) = \frac{1}{s^2 + A(s)V_s(s)C(s)} v^2 \rho(s). \quad (4.5)$$

In order to prevent excessive steering oscillation, sufficient phase margin (pm) and gain margin (gm) are required for the above system:

$$\angle \frac{A(j\omega_p)V_s(j\omega_p)C(j\omega_p)}{\omega_p^2} > -(\pi - pm), \quad \text{at} \quad \left| \frac{A(j\omega_p)V_s(j\omega_p)C(j\omega_p)}{\omega_p^2} \right| = 1; \quad (4.6)$$

as well as

$$\left| \frac{A(j\omega_g)V_s(j\omega_g)C(j\omega_g)}{\omega_g^2} \right| < \frac{1}{gm}, \quad \text{at} \quad \angle \frac{A(j\omega_g)V_s(j\omega_g)C(j\omega_g)}{\omega_g^2} = -\pi. \quad (4.7)$$

In order to maintain a tight lane-keeping ability, the following lane-tracking requirement is imposed:

$$|\Delta y_s(t)| \leq K_a \max(v^2 | \rho |). \quad (4.8)$$

The requirement in Eq. (4.8) guarantees that the lateral displacement deviation (Δy_s) shall not exceed K_a meters from a 1 m/s^2 step input of the reference road acceleration ($v^2 \rho$). By using the inequality

$$|\Delta y_s(t)| = L^{-1} \left\{ \frac{1}{s^2 + A(s)V_s(s)C(s)} \frac{v^2 \rho}{s} \right\} \leq \sup_{s=j\omega} \left(\left| \frac{1}{s^2 + A(s)V_s(s)C(s)} \right| \right) \max(v^2 \rho) \quad (4.9)$$

where L^{-1} denotes the inverse *Laplace* transform, Eq. (4.9) can be rewritten as

$$\left| \frac{1}{s^2 + A(s)V_s(s)C(s)} \right|_{s=j\omega} \leq K_a. \quad (4.10)$$

Eqs. (4.6), (4.7) and (4.10) are the basic design requirements for the controller $C(s)$.

4.2.2 Look-ahead Steering Controller

According to Eq. (4.4), the “look-ahead” distance d_s can be regarded as an additional “control parameter” along with the parameters of $C(s)$. To investigate the effects of this extra degree of freedom with respect to the steering controller design, the simple closed-

loop structure with two constant control gains (d_s and $C(s) = k_c$) is chosen at any given vehicle velocity in this section as

$$\Delta y_s(s) = \frac{1}{s^2 + A(s)V_S(s, d_s)k_c} v^2 \rho(s). \quad (4.11)$$

The following optimization technique is then derived to obtain the optimal control gains that attain the closed-loop requirements in (4.6), (4.7) and (4.10):

For every vehicle speed v and for any given d_s , the maximum attainable phase margin, $\beta_{\max}(d_s, v)$, is obtained as

$$\beta_{\max}(d_s, v) = \max_{\omega \in R, \left| \frac{A(j\omega_g)V_S(j\omega_g, d_s, v)\omega_p^2}{A(j\omega_p)V_S(j\omega_p, d_s, v)\omega_g^2} \right| \leq \frac{1}{gm}} \left(\angle(A(j\omega)V_S(j\omega, d_s, v)) \right), \quad (4.12)$$

where the frequencies ω_p and ω_g are determined by

$$\angle(A(j\omega_g)V_S(j\omega_g, d_s, v)) = 0, \quad (4.13)$$

$$\beta_{\max}(d_s, v) = \angle(A(j\omega_p)V_S(j\omega_p, d_s, v)). \quad (4.14)$$

The local optimal choice of k_c that results in the maximum attainable phase margin, $\beta_{\max}(d_s, v)$, for a given d_s is defined by

$$k'_c(d_s, v) = \left| \frac{-\omega_p^2}{A(j\omega_p)V_S(j\omega_p, d_s, v)} \right|. \quad (4.15)$$

The optimal choice of the control gain pair $(\bar{k}_c(v), \bar{d}_s(v))$ that satisfies the stability requirements (4.6) and (4.7) for any given vehicle speed v is calculated as

$$\bar{k}_c(v) = \max_{d_s \in R, \beta_{\max}(d_s, v) > pm} (k'_c(d_s, v)) = k'_c(\bar{d}_s(v), v). \quad (4.16)$$

Finally, the lane-tracking performance is examined by using Eqs. (4.10) and (4.16) as

$$\left| \frac{1}{s^2 + A(s)V_S(s, \bar{d}_s(v), v)\bar{k}_c(v)} \right|_{s=j\omega} \leq K_a(v). \quad (4.17)$$

Since Eq. (4.17) provides a conservative estimate, a more precise error bound can be obtained by directly computing the maximum transient error with respect to a 1 m/s^2 step road acceleration input through the inverse Laplace transformation.

Figure 4.4 displays the optimal control gain pair $(\bar{k}_c(v), \bar{d}_s(v))$ computed by Eqs. (4.12) to (4.16), as well as the resultant maximum transient error and error bound (K_a by Eq. (4.17)). The optimal gain pairs guarantee at least 50-degree phase margin (pm is set for 50 degrees in the above computations) and gain margin of 6 db for every vehicle speed. Initial observation of Figure 4.4(a) reveals three phenomena that follow engineering intuition: (1) the optimal look-ahead distance increases as the speed increases; (2) the larger the look-ahead distance, the smaller the feedback gain; (3) large feedback gain is required at very low vehicle speeds. According to Figure 4.4, a look-ahead distance of about 1 to 2 car-length is generally adequate for steering control. It is straightforward to show that the smoothness of the optimal gain curves improves the robustness of the “gain-scheduling” algorithm with respect to speed variations.

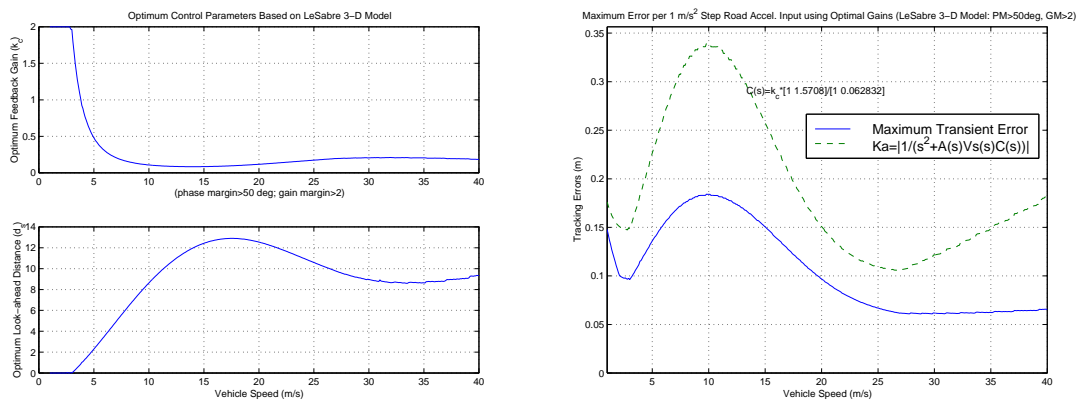


Fig. 4. Optimal control gain pair (\bar{k}_c, \bar{d}_s) and resultant maximum transient error based on 3 DOF model with constant control parameters ($pm=50$ deg, $gm=2$)
(a) Left: (\bar{k}_c, \bar{d}_s) ; (b) Right: K_a and maximum transient error.

Figure 4.4(b) illustrates the lane-tracking ability of the optimal gain pairs. The gain pairs result in 18 cm maximum tracking error (including transient) for every 0.1g lateral road disturbance without any prior knowledge of road curvature. It demonstrates the possibility of using constant feedback gain with constant look-ahead distance to achieve all lane-tracking requirements specified in Section 4.1.1 at any speed.

4.2.3 Optimal Frequency-Shaped Look-ahead Steering Controller

The results in Section 4.2.2 imply that a simple controller combining constant feedback gain and constant look-ahead distance may achieve all performance requirements described in Section 4.1.1. However several practical constraints limit the feasibility of such simple implementation. The amplification of the measurement noise limits the length of the look-ahead distance to a couple of car length; high feedback gain with large look-ahead distance can easily excite the non-linearity or unmodeled dynamics in the steering actuators or mechanism; large look-ahead distance creates noticeable steady state tracking error during curves.

In order to address both the practical limitations and the specific phase lead requirement associated with the constant look-ahead distance depicted in Section 4.2.2, a frequency shaped look-ahead controller law is proposed as

$$V_s(s) = sG_{\dot{y}_r, \delta}(s) + d_s(v)G_{d_s}(s)sG_{\dot{\psi}, \delta}(s) + h_s sG_{\dot{\phi}, \delta}(s), \quad (4.18)$$

along with a feedback compensator that mainly compensates for the actuator dynamics:

$$C(s) = k_c(v)G_c(s). \quad (4.19)$$

Following the design philosophy of minimum controller transition, two speed-independent filters, $G_{d_s}(s)$ and $G_c(s)$, are chosen for investigation in this section. In order to reduce both the effects of the steady state tracking bias and the unwanted excitation of the high frequency unmodeled actuator dynamics, $G_c(s)$ consists of a low-frequency integrator and high-frequency roll-off. Similarly, $G_{d_s}(s)$ is made of a high frequency roll-off portion and a mid-frequency lead-lag filter to limit the look-ahead amplification and to provide extra “look-ahead” between 0.5 and 2 Hz. In this section, these two additional control filters are chosen as

$$G_c(s) = \frac{25\pi(s + 0.5\pi)}{(s + 0.02\pi)(s + 25\pi)} \quad (4.20)$$

$$G_{d_s}(s) = \frac{20\pi(s + 0.4\pi)}{(s + 0.8\pi)(s + 10\pi)} \quad (4.21)$$

Inserting $G_{d_s}(s)$ into $V_s(s)$ as in Eq. (4.18) and appending $G_c(s)$ to all open-loop transfer functions immediately after $V_s(s)$ for Eqs. (4.12) to (4.15), the corresponding optimal

control gain pair $(\bar{k}_c(v), \bar{d}_s(v))$ that satisfies the stability requirements (4.6) and (4.7) for any given vehicle speed v is calculated as in Eqs. (4.12) to (4.16).

The optimal control gain pair $(\bar{k}_c(v), \bar{d}_s(v))$ corresponding to the control filters $(G_c(s), G_{ds}(s))$, as well as the resultant maximum transient error and error bound (K_a) are plotted in Figure 4.5. Similarly, the optimal gain pairs guarantee at least 50 degrees phase margin and 6 db gain margin for any vehicle speed. As the result of the additional phase lead created by the larger look-ahead distance between 0.5 and 3 Hz, the frequency-shaped look-ahead scheme renders a more desirable optimal gain pair characteristics. Generally speaking, the look-ahead distance increases and the feedback gain decreases as the vehicle speed increases. More specifically, $(\bar{k}_c(v), \bar{d}_s(v))$ remain almost constant for vehicle speeds between 15 and 30 m/s. This indicates that a “constant” controller can work almost optimally from medium to highway speeds. The relatively “flat” gains with respect to velocity also imply that the controller has high tolerance to velocity errors.

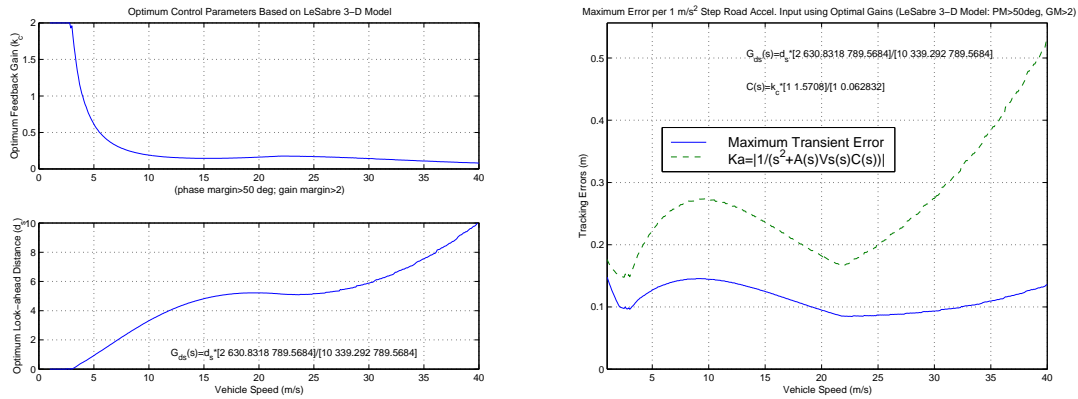


Fig. 5. Optimal control gain pair (\bar{k}_c, \bar{d}_s) and resultant maximum transient error based on 3 DOF model with frequency shaped look-ahead control ($pm=50$ deg, $gm=2$)
(a) Left: (\bar{k}_c, \bar{d}_s) ; (b) Right: K_a and maximum transient error.

Figure 4.5(b) shows that the resultant maximum tracking error (including transient) is less than 15 cm for every 0.1g lateral road disturbance without any prior knowledge of road curvature. It satisfies all lane-tracking requirements specified in Section 4.1.1 at any speed.

4.2.4 Final Controller Implementation

Section 4.2.3 provides strong arguments for implementing the frequency-shaped look-ahead steering controller in practice: simple, robust and satisfying performance requirements. Eqs. (4.18) and (4.19) can be directly adopted for controller design when the yaw angle measurement is available. On the other hand, when the vehicle uses a “look-down” lateral sensing system for lateral control, the yaw angle can be estimated by a second “look-down” measurement. Under the assumption that the distances from all sensors to roll axis are about the same, the yaw angle can be easily approximated as

$$\psi \cong \frac{y_f - y_b}{L} \quad (4.22)$$

where y_f and y_b are the lateral measurements in front and back of the vehicle, respectively, and L is the distance between these two sensors.

The final steering control algorithm implemented in the test vehicle needs to satisfy both tracking accuracy and ride comfort requirements for all operational scenarios discussed in Section 4.1.1 at various vehicle speeds regardless of the following uncertainties: road adhesion variations, incorrect road curvature information, sensor noises, actuator bandwidth, vehicle dynamics changes, soft suspension modes, and vehicle parameters. Using the analysis results from this report with some tuning in the vehicle, the following final frequency shaped virtual look-ahead lane-keeping control algorithm was developed and implemented:

$$\delta_c = -k_c(v)G_c(s)(k_{int}(s)y + d_s(v)G_{ds}(s)\psi) \quad (4.23)$$

where δ_c is the steering command, k_{int} an additional integrator to keep the steady state tracking error small, G_{ds} the virtual sensor look-ahead filter, G_c the compensator at the virtual sensor location. The two gain-scheduled coefficients, $k_c(v)$ and $d_s(v)$, follow the velocity dependent relationships from Figure 4.5(a).

5. References

1. Peng, H. and Tomizuka, M., "Preview Control for Vehicle Lateral Guidance in Highway Automation." *ASME Journal of Dynamic Systems, Measurement and Control*, vol. 115, no. 4, pp. 678-686, 1993.
2. Aso, M. and Suzuki, T., "Automated Steering Control for the Intelligent Multimode Transit System," *Proceedings of the IEEE Intelligent Vehicles Symposium 2000*, Dearborn, MI, USA, pp. 590-595.
3. O'Brien, O. T., Iglesias, P. A. and Urban, T. J., "Vehicle Lateral Control for Automated Highway Systems," *IEEE Transactions on Control Systems Technology*, vol. 4, no. 3, May 1996, pp. 266-273.
4. Hingwe, P., Tan, H.-S., Packard, A. K. and Tomizuka, M., "Linear parameter varying controller for automated lane guidance experimental study on tractor semi-trailers," to appear in *IEEE Transactions on Control Systems Technology*, 2002.
5. Fenton, R. E. and Mayhan, R. J., "Automated highway studies at The Ohio State University - an overview," *IEEE Transactions on Vehicular Technology*, VT-40(1), 1991, pp. 100-113.
6. Guldner, J., Tan, H.-S. and Patwardhan, S., "Analysis of Automatic Steering Control for Highway Vehicle with Look-down Lateral Reference Systems," *Vehicle System Dynamics*, vol. 26, no. 4, 1996, pp. 243-269.
7. Guldner, J., Sienel, W., Tan, H.-S., Ackermann, J., Patwardhan, S. and Bunte, T., "Robust Automatic Steering Control for Look-Down Reference Systems with Front and Rear Sensors," *IEEE Transactions on Control Systems Technology*, vol. 7, no. 1, Jan. 1999, pp. 2-11.
8. Smith, D., Benton, R. and Starkey, J., "Nonlinear-gain-optimized Controller Development and Evaluation for Automated emergency Vehicle Steering," *International Journal of Vehicle Design*, vol. 24, no. 1, 2000, pp. 79-99.
9. Chen, C. and Tomizuka, M., "Lateral control of commercial heavy vehicles," *Vehicle System Dynamics*, vol. 33, no. 6, June 2000, pp. 391-420.
10. Hingwe, P. and Tomizuka, M., "Experimental evaluation of a chatter free sliding mode control for lateral control in AHS," *Proceedings of the 1997 American Control Conference*, Albuquerque, NM, USA, 1997, pp. 3365-3369.

11. Yamamoto, M., Kagawa, Y. and Okuno, A., "Robust Control for Automated Lane Keeping Against Lateral Disturbance," *Proceedings 1999 IEEE/IEEJ/JSAI International Conference on Intelligent Transportation Systems*, Tokyo, Japan, 1999, pp. 240-245.
12. Choi, S. B., "The Design of a Look-down Feedback Adaptive Controller for the Lateral Control of Front-wheel-steering Autonomous Highway Vehicles," *IEEE Transactions on Vehicular Technology*, vol. 49, no. 6, Nov. 2000, pp. 2257-2269.
13. Byrne, R. H. and Abdallah, C. T., "Design of a Model Reference Adaptive Controller for Vehicle Road Following," *Mathematical and Computer Modelling*, vol. 22, no. 4-7, 1995, pp. 343-354.
14. Feng, K.-T., Tan, H.-S. and Tomizuka, M., "Automatic Steering Control and Validation of Vehicle Lateral Motion with the Effect of Roll Dynamics," *Proceedings of American Control Conference*, Philadelphia, PA, USA, June 1998, pp. 2248-2252.